

Temperature and thermal stress distributions in a hollow circular cylinder composed of anisotropic and isotropic materials

Mohammad Javad Namayandeh¹, Mehdi Mohammadimehr^{*1},
Mojtaba Mehrabi¹ and Abbas Sadeghzadeh-Attar²

¹ Department of Solid Faculty of Mechanical Engineering, University of Kashan, Kashan, Iran

² Department of Metallurgy and Materials Engineering, University of Kashan, Kashan, Iran

(Received June 23, 2019, Revised January 21, 2020, Accepted February 29, 2020)

Abstract. In this article, an analytical solution is presented for the steady-state axisymmetric thermal stress distributions in a composite hollow cylinder. The cylinder is composed of two isotropic and anisotropic materials which is subjected to the thermal boundary conditions of convective as well as radiative heating and cooling on the inner and outer surfaces, respectively. The solution of the temperature is obtained by means of Bessel functions and the thermal stresses are developed using Potential functions of displacement. Numerical results are derived for a cylinder which is similar to a gas turbine combustor and showed that the maximum temperature and thermal stresses (radial, hoop, axial) occurred in the middle point of cylinder and the values of thermal stresses in anisotropic cylinder are more than the isotropic cylinder. It is worthy to note that the values of the thermal conditions which estimated in this research, not to be presented in any other papers but these values are very accurate in calculation.

Keywords: anisotropic and isotropic materials; hollow cylinder; thermal stresses; bessel functions; potential function displacements; steady-state

1. Introduction

Thermal stresses in scientific studies are one of the important topics in mechanical engineering and have received considerable attention both in analysis and design. These stresses induced when differential thermal expansions are caused in a cylinder body, and if these stresses are high and associated with high temperatures in the body, yield stress of the material at these temperatures may be approached or even exceeded. There are some researches which have investigated on the thermal stresses in cylinders. For example, it is well known that in aerospace and nuclear engineering, many structural components are subjected to severe thermal loadings which give rise to intense thermal stresses in the components, especially near cracks and other kinds of defects (Xue *et al.* 2018). The high thermal stresses around defects may cause catastrophic failure of the cracked structure (Jin and Noda 1994). There are many researches in this field that considered the effect of thermal stresses on the behaviors of structures and predicted the response of them against the effects of various distributions. In this section presented some of these studies such as:

Analytical solutions for the thermal stresses in a hollow cylinder with the convective boundary

*Corresponding author, Ph.D., Associate Professor, E-mail: mmohammadimehr@kashanu.ac.ir

conditions on the inside and outside surfaces considered by Aziz and Torabi (2013). They investigated one dimensional steady conduction in the radial direction with uniform internal heat generation and assumed the radial stresses on the inside and the outside surfaces to be zero. Mohammadimehr and Mehrabi (2017, 2018a) studied thermal stability and vibration analyses of two double-bonded cylindrical shells reinforced by nanocomposite carbon nanotube. They showed that temperature distribution lead to change natural frequencies and stability of their structures. Mahmoudi and Atefi (2012), obtained the heat conduction equation and the associated thermal stresses are obtained in a hollow cylinder of homogenous and isotropic material using transient Fourier series. Their considered cylinder was under a periodic time-varying thermal loading in the inner circular, insulated on the outer circular surfaces and constant temperature of two other faces. They found that the depth of penetration of temperature fluctuation and related thermal stresses highly depend on the period of oscillation of thermal loading and thermo physical properties of the cylinder. Namayandeh *et al.* (2019) considered a simplified model of alumina ceramic to obtain the temperature distribution of a V94.2 gas turbine combustor under realistic operation conditions. The external thermal loads consist of convection and radiation heat transfers are considered that these loads are applied to flat segmented panel on hot side and forced convection cooling on the other side. Liu and Yin (2014) investigated the thermal elastic fields in the hollow circular overlay fully bonded to a rigid substrate, which is subjected to a temperature change. They showed that their results are useful for thermal stress analysis of the hollow circular thin film/substrate systems and for fracture analysis of spiral cracking. A nonlinear thermoelastic analysis of a thick-walled cylinder made of functionally graded material is performed by Moosaie (2016). He discussed about temperature field, material properties and radial stress versus the radial direction. Using closed-form exact solution, Zenkour (2014) predicted the hygro-thermal response of inhomogeneous piezoelectric hollow cylinders. He illustrated that the inhomogeneity parameter, the pressure load ratio, the electric potential ratio, the initial temperature, and the final concentration have significant effects on the temperature, moisture, displacement, stresses, and electric potential. Yaragal and Ramanjaneyulu (2016) investigated the effect of elevated temperature on the mechanical properties of the concrete specimen with polypropylene fibres and cooled differently under various regimes. Dejean and Mohr (2018) introduced a new family of elastically-isotropic elementary cubic truss lattice structures, eliminating the need of combining elementary structures to achieve elastic isotropy. Zibdeh and Al Farran (1995) presented a steady-state solution for the thermal stresses of a homogeneous, orthotropic hollow cylinder subjected to an asymmetric temperature distribution on the outer surface and heat convection on the inner surface. They derived the thermal stresses and displacements for single and multilayer cylinders with fiber oriented 0, 90, 180 deg. using three-dimensional linear elasticity approach. Their numerical results indicated that the single-layer, 0-deg cylinder has the lowest value of stresses and so the thermal stresses increase as the thickness increases. Yee and Moon (2002) employed Fourier–Bessel expansions and stress function methods to analysis the transient, plane thermal stresses of a linearly elastic, homogeneously orthotropic hollow cylinder subjected to an arbitrary temperature distribution. One of the most their research results showed that the thermal stress distributions were greatly affected by the thermal boundary and initial conditions. Lee (2005) solved the transient and steady-state thermal stresses in a multilayered hollow cylinder under periodic loading conditions using Laplace transform and finite difference methods.

Some researchers worked about sandwich, composite and nanocomposite structures in thermal environment. Ghorbanpour Arani *et al.* (2016) depicted surface stress and agglomeration effects on nonlocal biaxial buckling polymeric nanocomposite plate reinforced by CNT using various

approaches. Mohammadimehr and Rostami (2018b) illustrated bending and vibration analysis of a rotating sandwich cylindrical shell by considering nanocomposite core and piezoelectric layers under thermal and magnetic fields. Shahedi and Mohammadimehr (2019) presented vibration behavior of rotating fully-bonded and delaminated sandwich beam with CNTRC face sheets and AL-foam flexible core in thermal and moisture environments. In the other work, they (Shahedi and Mohammadimehr 2020) considered nonlinear high-order dynamic stability of AL-foam flexible cored sandwich beam with variable mechanical properties and carbon nanotubes-reinforced composite face sheets in thermal environment. Bamdad *et al.* (2019) considered buckling and vibration analysis of sandwich Timoshenko porous beam with temperature-dependent material properties under magneto-electro-elastic loadings. Rajabi and Mohammadimehr (2019) investigated hydro-thermo-mechanical biaxial buckling analysis of sandwich micro-plate with isotropic/orthotropic cores and piezoelectric/polymeric nanocomposite face sheets based on FSDT on elastic foundations. Mohammadimehr *et al.* (2017) showed dynamic stability of modified strain gradient theory sinusoidal viscoelastic piezoelectric polymeric functionally graded single-walled carbon nanotubes reinforced nanocomposite plate considering surface stress and agglomeration effects under hydro-thermo-electro-magneto-mechanical loadings. Thermal bifurcation buckling behavior of fully clamped Euler-Bernoulli nanobeam built of a through thickness functionally graded material is explored by Bensaid and Bekhadda (2018). They illustrated that the critical buckling load decrease with increasing temperature changes.

Many papers have analyzed the temperature and thermal stress distributions in cylinders, but a cylinder which is composed of anisotropic and isotropic materials hasn't considered, yet and it is the novelty of this research. This persuade us to study this issue because of its importance in major industries such as power plants. Therefore, in this paper, the steady-state temperature and thermal stress distributions are analyzed in a finite hollow circular cylinder composed of two different anisotropic and isotropic, homogeneous materials which is heated by convection and radiation on the inner surface and cooled by convection and radiation on the outer surface. The cylinder is simply supported on its two ends. The mechanical and thermal loads are axisymmetric. Because of complexity of modeling the radiation, it is considered as a constant heat rate of q_1'' , q_2'' on the internal and external surfaces, respectively. It is worthy to note that the values of the thermal conditions which estimated in this research, not to be presented in any other papers but they are very accurate in calculation.

2. Mathematical model

Consider a hollow cylinder of finite length L , inner radius r_1 and outer radius r_2 as shown in Fig. 1. It is composed of two anisotropic and isotropic homogenous materials and simply supported at two ends where the temperature of them is T_0 . The internal surface is heated by a fluid at the temperature of T_∞ and the convective coefficient of h_1 as well as a heat radiation of q_1'' . However, the external surface is subjected to the cooling flow due to a heat convection which is created by the same fluid but with the temperature of T_0 and convective coefficient of h_2 along with a heat radiation of q_2'' . Axisymmetric steady-state boundary conditions and cylindrical coordinates (r, θ, z) are considered.

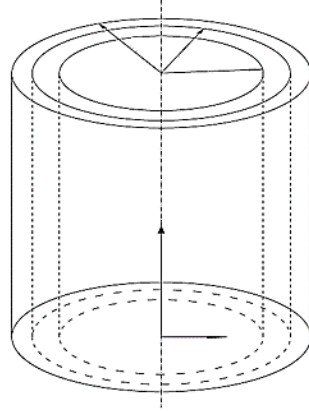


Fig. 1 Geometrical model of composite hollow cylinder

3. Heat conduction

The heat conduction equation for the 2-D steady-state temperature field and no heat generation in an anisotropic hollow cylinder is as follows (Misra and Achari 1980)

$$\left[k_r \frac{\partial}{\partial r} \left(\frac{\partial}{\partial r} + \frac{1}{r} \right) + k_z \frac{\partial^2}{\partial z^2} \right] T_1(r, z) = 0 \quad r_1 \leq r \leq r_2, \quad 0 \leq z \leq L \quad (1)$$

where $T_1(r, z)$ is the temperature distribution and k_r and k_z are the thermal conductivities in the radial and axial directions, respectively.

Considering $k_r = k_z$, the Eq. (1) for the temperature distribution $T_2(r, z)$ in an isotropic cylinder can be expressed as

$$\left[\frac{\partial}{\partial r} \left(\frac{\partial}{\partial r} + \frac{1}{r} \right) + \frac{\partial^2}{\partial z^2} \right] T_2(r, z) = 0 \quad r_2 \leq r \leq r_3, \quad 0 \leq z \leq L \quad (2)$$

Thermal boundary conditions are assumed as follows

$$T_1(r, z) = T_2(r, z) = T_0 \quad z = 0, \quad z = L \quad (3)$$

$$-k_1 \frac{\partial T_1}{\partial r} = h_1(T_\infty - T_1(r, z)) - q_1'' \quad r = r_1 \quad (4)$$

$$-k(r) \frac{\partial T_2}{\partial r} = h_2(T_2(r, z) - T_0) + q_2'' \quad r = r_3 \quad (5)$$

$$T_1(r, z) = T_2(r, z) \quad r = r_2 \quad (6)$$

$$k_1 \frac{\partial T_1}{\partial r} = k_r \frac{\partial T_2}{\partial r} \quad r = r_2 \quad (7)$$

In order to simplify of the problem, the following parameters are defined (Eslami and Hetnarski 2013)

$$k^2 = \frac{k(z)}{k(r)}, \quad k_3 = \frac{k_1}{k_r}, \quad H_1 = \frac{h_1}{k_1}, \quad H_2 = \frac{h_2}{k_r}, \quad \theta_i = T_i(r, z) - T_0, \quad i = 1, 2, \quad \theta_\infty = T_\infty - T_0 \quad (8)$$

Applying parameters Eq. (8), Eq. (1) to Eq. (7) considered as follows

$$\left[\frac{\partial}{\partial r} \left(\frac{\partial}{\partial r} + \frac{1}{r} \right) + k^2 \frac{\partial^2}{\partial z^2} \right] \theta_1(r, z) = 0 \quad r_1 \leq r \leq r_2, \quad 0 \leq z \leq L \quad (9)$$

$$\left[\frac{\partial}{\partial r} \left(\frac{\partial}{\partial r} + \frac{1}{r} \right) + \frac{\partial^2}{\partial z^2} \right] \theta_2(r, z) = 0 \quad r_2 \leq r \leq r_3, \quad 0 \leq z \leq L \quad (10)$$

$$\theta_1(r, z) = \theta_2(r, z) = 0 \quad z = 0, \quad z = L \quad (11)$$

$$\frac{\partial \theta_1}{\partial r} = H_1(\theta_1(r, z) - \theta_\infty) + q_1 \quad r = r_1 \quad (12)$$

$$\frac{\partial \theta_2}{\partial r} = -[H_2(\theta_2(r, z)) + q_2] \quad r = r_3 \quad (13)$$

$$\theta_1(r, z) = \theta_2(r, z) \quad r = r_2 \quad (14)$$

$$k_3 \frac{\partial \theta_1}{\partial r} = \frac{\partial \theta_2}{\partial r} \quad r = r_2 \quad (15)$$

Using the method of the separation of variables and the boundary conditions (11), the solutions for $\theta_1(r, z), \theta_2(r, z)$ can be written as follows

$$\theta_1(r, z) = \sum_{n=1}^{\infty} [C_{1n} \cdot I_0(\alpha_{n1} r) + D_{1n} \cdot K_0(\alpha_{n1} r)] \sin\left(\frac{\alpha_{n1}}{k} z\right) \quad (16)$$

$$\theta_2(r, z) = \sum_{n=1}^{\infty} [C_{2n} \cdot I_0(\alpha_{n2} r) + D_{2n} \cdot K_0(\alpha_{n2} r)] \sin(\alpha_{n2} z) \quad (17)$$

in which I_0 and k_0 are zero-order modified Bessel functions of the first and second kinds, respectively. and

$$\alpha_{n1} = \frac{n\pi k}{L} \quad (18)$$

$$\alpha_{n2} = \frac{n\pi}{L} \quad (19)$$

where $n = 1, 2, \dots$

$C_{1n}, D_{1n}, C_{2n}, D_{2n}$ are the constants which determined from the boundary conditions (12)-(15) that is shown in Appendix A.

4. Thermal stresses in the anisotropic cylinder

In the cylindrical coordinate, the stress-strain relations for an anisotropic material having elastic symmetry about z-axis are given by (Misra and Achari 1980)

$$\begin{aligned}\sigma_{rr} &= C_{11}\varepsilon_r + C_{12}\varepsilon_\theta + C_{13}\varepsilon_z - \beta_1\theta_1 \\ \sigma_{\theta\theta} &= C_{12}\varepsilon_r + C_{11}\varepsilon_\theta + C_{13}\varepsilon_z - \beta_1\theta_1 \\ \sigma_{zz} &= C_{13}\varepsilon_r + C_{13}\varepsilon_\theta + C_{33}\varepsilon_z - \beta_2\theta_1 \\ \tau_{rz} &= C_{44}\gamma_{rz}\end{aligned}\quad (20)$$

in which σ_{ij}, τ_{ij} are the stress components, C_{ij} are the elastic constants and

$$\begin{aligned}\varepsilon_r &= \frac{\partial u(r, z)}{\partial r}, \quad \varepsilon_\theta = \frac{u(r, z)}{r}, \quad \varepsilon_z = \frac{\partial w(r, z)}{\partial z}, \quad \gamma_{rz} = \frac{\partial u(r, z)}{\partial z} + \frac{\partial w(r, z)}{\partial r} \\ \beta_1 &= (C_{11} + C_{12})\alpha_r + C_{13}\alpha_z, \quad \beta_2 = 2C_{13}\alpha_r + C_{33}\alpha_z\end{aligned}\quad (21)$$

where $u(r, z), w(r, z)$ are the radial and axial displacements and α_r, α_z are the thermal expansion coefficients along the radial and axial directions, respectively.

The non-vanishing equations of equilibrium in the cylindrical coordinate and the absence of body forces are considered as follows:

$$\frac{\partial \sigma_{rr}}{\partial r} + \frac{\partial \tau_{rz}}{\partial z} + \frac{\sigma_{rr} - \sigma_{\theta\theta}}{r} = 0, \quad \frac{\partial \tau_{rz}}{\partial r} + \frac{\partial \sigma_z}{\partial z} + \frac{1}{r}\tau_{rz} = 0 \quad (22)$$

Substituting relations (20) into Eq. (22) we have (Misra and Achari 1980)

$$C_{11} \left(\frac{\partial^2 u}{\partial r^2} \right) + \left(\frac{1}{r} \frac{\partial u}{\partial r} - \frac{u}{r^2} \right) + [C_{13} + C_{44}] \frac{\partial^2 w}{\partial r \partial z} + C_{44} \frac{\partial^2 u}{\partial z^2} = \beta_1 \frac{\partial \theta_1}{\partial r} \quad (23)$$

$$C_{44} \left(\frac{\partial^2 w}{\partial r^2} + \frac{1}{r} \frac{\partial w}{\partial r} \right) + [C_{13} + C_{44}] \left(\frac{\partial^2 u}{\partial r \partial z} + \frac{1}{r} \frac{\partial u}{\partial z} \right) + C_{33} \frac{\partial^2 w}{\partial z^2} = \beta_2 \frac{\partial \theta_1}{\partial z} \quad (24)$$

In order to solve Eqs. (23) and (24) we assume

$$u(r, z) = \frac{\partial}{\partial r} (\phi + \psi), \quad w(r, z) = \frac{\partial}{\partial z} (\lambda\phi + \mu\psi) \quad (25)$$

where ϕ, ψ are the displacement potential functions of r, z and λ, μ being arbitrary constants.

Using functions (25) and from Eq. (23) to Eq. (24), we have

$$C_{11} \left(\frac{\partial^2 \phi}{\partial r^2} + \frac{1}{r} \frac{\partial \phi}{\partial r} \right) + [C_{44} + \lambda(C_{13} + C_{44})] \frac{\partial^2 \phi}{\partial z^2} = 0 \quad (26)$$

$$C_{11} \left(\frac{\partial^2 \psi}{\partial r^2} + \frac{1}{r} \frac{\partial \psi}{\partial r} \right) + [C_{44} + \mu(C_{13} + C_{44})] \frac{\partial^2 \psi}{\partial z^2} = \beta_1 \theta_1 \quad (27)$$

$$[C_{13} + (1 + \lambda)C_{44}] \left(\frac{\partial^2 \phi}{\partial r^2} + \frac{1}{r} \frac{\partial \phi}{\partial r} \right) + \lambda C_{33} \frac{\partial^2 \phi}{\partial z^2} = 0 \quad (28)$$

$$[C_{13} + (1 + \mu)C_{44}] \left(\frac{\partial^2 \psi}{\partial r^2} + \frac{1}{r} \frac{\partial \psi}{\partial r} \right) + \mu C_{33} \frac{\partial^2 \psi}{\partial z^2} = \beta_2 \theta_1 \quad (29)$$

Using Eq. (16), we take

$$\psi(r, z) = \sum_{n=1}^{\infty} [C_{1n} \cdot P_n \cdot I_0(\alpha_{n1}r) + D_{1n} \cdot Q_n \cdot K_0(\alpha_{n1}r)] \sin\left(\frac{\alpha_{n1}}{k}z\right) \quad (30)$$

in which P_n, Q_n are arbitrary functions of α_{n1} to be obtained from the Eq. (26) and Eq. (29) as follows

$$\begin{aligned} \alpha^2_{n1} \cdot P_n [k^2 C_{11} - (C_{44} + \mu(C_{13} + C_{44}))] &= \beta_1 k^2 \\ \alpha^2_{n1} \cdot P_n [(C_{13} + (1 + \mu)C_{44})k^2 - \mu C_{33}] &= \beta_2 k^2 \end{aligned} \quad (31)$$

$$\begin{aligned} \alpha^2_{n1} \cdot Q_n [k^2 C_{11} - (C_{44} + \mu(C_{13} + C_{44}))] &= \beta_1 k^2 \\ \alpha^2_{n1} \cdot Q_n [(C_{13} + (1 + \mu)C_{44})k^2 - \mu C_{33}] &= \beta_2 k^2 \end{aligned} \quad (32)$$

Then

$$\mu = \frac{\beta_2(k^2 C_{11} - C_{44}) - \beta_1 k^2 (C_{13} + C_{44})}{\beta_2 (C_{13} + C_{44}) + \beta_1 (k^2 C_{44} - C_{33})} \quad (33)$$

and

$$P_n = Q_n = \alpha_{n1}^{-2} \frac{\beta_1 k^2 (k^2 C_{44} - C_{33}) + \beta_2 k^2 (C_{13} + C_{44})}{k^2 (C_{13} + C_{44})^2 + (k^2 C_{44} - C_{33})(k^2 C_{11} - C_{44})} \quad (34)$$

If the Eq. (26) and Eq. (28) to give a non-zero solution, simultaneously, we must have

$$\frac{\lambda C_{13} + (1 + \lambda)C_{44}}{C_{11}} = \frac{\lambda C_{33}}{C_{13} + (1 + \lambda)C_{44}} = S^2 \text{ (say)} \quad (35)$$

Substituting Eq. (35) into Eqs. (26) and (27) yields the following equation

$$\frac{\partial^2 \phi}{\partial r^2} + \frac{1}{r} \frac{\partial \phi}{\partial r} + S^2 \frac{\partial^2 \phi}{\partial z^2} = 0 \quad (36)$$

Then, the Eq. (36) has two solutions of $\phi_1(r, z), \phi_2(r, z)$ corresponding to the two values of S^2 which are the roots of the equation (Lenkhmitskii 1981)

$$C_{11} C_{44} S^4 + (C^2_{13} + 2C_{13} C_{44} - C_{11} C_{33}) S^2 + C_{33} C_{44} = 0 \quad (37)$$

Finally, to derive stress components, we define $u(r, z), w(r, z)$ using displacement potential functions ϕ_1, ϕ_2, ψ as follows

$$u = \frac{\partial}{\partial r}(\phi_1 + \phi_2 + \psi) \quad (38)$$

$$w = \frac{\partial}{\partial z}(\lambda_1 \phi_1 + \lambda_2 \phi_2 + \mu \psi) \quad (39)$$

where λ_1, λ_2 are the values of λ corresponding to the two different values of S^2 in Eq. (35).

As solutions of Eq. (36) for ϕ_1, ϕ_2 we can take

$$\phi_1(r, z) = \sum_{n=1}^{\infty} \left[C_{1n} \cdot E_{1n} \cdot I_0 \left(\frac{\alpha_{n1} S_1}{k} r \right) + D_{1n} \cdot F_{1n} \cdot K_0 \left(\frac{\alpha_{n1} S_1}{k} r \right) \right] \sin \left(\frac{\alpha_{n1}}{k} z \right) \quad (40)$$

$$\phi_2(r, z) = \sum_{n=1}^{\infty} \left[C_{1n} \cdot E_{2n} \cdot I_0 \left(\frac{\alpha_{n1} S_2}{k} r \right) + D_{1n} \cdot F_{2n} \cdot K_0 \left(\frac{\alpha_{n1} S_2}{k} r \right) \right] \sin \left(\frac{\alpha_{n1}}{k} z \right) \quad (41)$$

where $E_{n1}, F_{n1}, E_{n2}, F_{n2}$ are arbitrary constant, to be determined from the mechanical boundary conditions.

Using Eqs. (20), (38), (39), the displacement and stress components for the anisotropic cylinder are given by

$$u(r, z) = k^{-1} \sum_{n=1}^{\infty} \alpha_{n1} \left[S_1 R'_{02} \left(\frac{\alpha_{n1} S_1}{k} r \right) + S_2 R'_{03} \left(\frac{\alpha_{n1} S_2}{k} r \right) + k R'_{04}(\alpha_{n1} r) \right] \sin \left(\frac{\alpha_{n1}}{k} z \right) \quad (42)$$

$$w(r, z) = k^{-1} \sum_{n=1}^{\infty} \alpha_{n1} \left[\lambda_1 R_{02} \left(\frac{\alpha_{n1} S_1}{k} r \right) + \lambda_2 R_{03} \left(\frac{\alpha_{n1} S_2}{k} r \right) + \mu R_{04}(\alpha_{n1} r) \right] \cos \left(\frac{\alpha_{n1}}{k} z \right) \quad (43)$$

$$\begin{aligned} \sigma_{rr} = k^{-2} \sum_{n=1}^{\infty} \{ & C_{11} \alpha_{n1}^2 \left[S_1^2 R''_{02} \left(\frac{\alpha_{n1} S_1}{k} r \right) + S_2^2 R''_{03} \left(\frac{\alpha_{n1} S_2}{k} r \right) + k^2 R''_{04}(\alpha_{n1} r) \right] \\ & + C_{12} \alpha_{n1} k r^{-1} \left[S_1 R'_{02} \left(\frac{\alpha_{n1} S_1}{k} r \right) + S_2 R'_{03} \left(\frac{\alpha_{n1} S_2}{k} r \right) + k R'_{04}(\alpha_{n1} r) \right] \\ & - C_{13} \alpha_{n1}^2 \left[\lambda_1 R_{02} \left(\frac{\alpha_{n1} S_1}{k} r \right) + \lambda_2 R_{03} \left(\frac{\alpha_{n1} S_2}{k} r \right) + \mu R_{04}(\alpha_{n1} r) \right] \\ & \left. - \beta_1 R_{01}(\alpha_{n1} r) \right\} \sin \left(\frac{\alpha_{n1}}{k} z \right) \end{aligned} \quad (44)$$

$$\begin{aligned} \sigma_{\theta\theta} = k^{-2} \sum_{n=1}^{\infty} \{ & C_{12} \alpha_{n1}^2 \left[S_1^2 R''_{02} \left(\frac{\alpha_{n1} S_1}{k} r \right) + S_2^2 R''_{03} \left(\frac{\alpha_{n1} S_2}{k} r \right) + k^2 R''_{04}(\alpha_{n1} r) \right] \\ & + C_{11} \alpha_{n1} k r^{-1} \left[S_1 R'_{02} \left(\frac{\alpha_{n1} S_1}{k} r \right) + S_2 R'_{03} \left(\frac{\alpha_{n1} S_2}{k} r \right) + k R'_{04}(\alpha_{n1} r) \right] \end{aligned} \quad (45)$$

$$\begin{aligned}
 & -C_{13}\alpha_{n1}^2 k^{-2} \left[\lambda_1 R_{02} \left(\frac{\alpha_{n1} S_1}{k} r \right) + \lambda_2 R_{03} \left(\frac{\alpha_{n1} S_2}{k} r \right) + \mu R_{04}(\alpha_{n1} r) \right] \\
 & -\beta_1 R_{01}(\alpha_{n1} r) \} \sin \left(\frac{\alpha_{n1}}{k} z \right)
 \end{aligned} \quad (45)$$

$$\begin{aligned}
 \sigma_{zz} = & k^{-2} \sum_{n=1}^{\infty} \{ C_{13}\alpha_{n1}^2 \left[S_1^2 R_{02}'' \left(\frac{\alpha_{n1} S_1}{k} r \right) + S_2^2 R_{03}'' \left(\frac{\alpha_{n1} S_2}{k} r \right) + k^2 R_{04}''(\alpha_{n1} r) \right] \\
 & + C_{13}\alpha_{n1} k r^{-1} \left[S_1 R_{02}' \left(\frac{\alpha_{n1} S_1}{k} r \right) + S_2 R_{03}' \left(\frac{\alpha_{n1} S_2}{k} r \right) + k R_{04}'(\alpha_{n1} r) \right] \\
 & - C_{33}\alpha_{n1}^2 \left[\lambda_1 R_{02} \left(\frac{\alpha_{n1} S_1}{k} r \right) + \lambda_2 R_{03} \left(\frac{\alpha_{n1} S_2}{k} r \right) + \mu R_{04}(\alpha_{n1} r) \right] \\
 & - \beta_2 R_{01}(\alpha_{n1} r) \} \sin \left(\frac{\alpha_{n1}}{k} z \right)
 \end{aligned} \quad (46)$$

$$\begin{aligned}
 \tau_{rz} = & C_{44} k^{-2} \sum_{n=1}^{\infty} \alpha_{n1}^2 \left\{ (S_1 + \lambda_1) R_{02}' \left(\frac{\alpha_{n1} S_1}{k} r \right) + (S_2 + \lambda_2) R_{03}' \left(\frac{\alpha_{n1} S_2}{k} r \right) \right. \\
 & \left. + k(1 + \mu) R_{04}'(\alpha_{n1} r) \right\} \cos \left(\frac{\alpha_{n1}}{k} z \right)
 \end{aligned} \quad (47)$$

in which

$$R_{01}(\alpha_{n1} r) = C_{1n} \cdot I_0(\alpha_{n1} r) + D_{1n} \cdot K_0(\alpha_{n1} r) \quad (48)$$

$$R_{02} \left(\frac{\alpha_{n1} S_1}{k} r \right) = C_{1n} \cdot E_{1n} \cdot I_0 \left(\frac{\alpha_{n1} S_1}{k} r \right) + D_{1n} \cdot F_{1n} \cdot K_0 \left(\frac{\alpha_{n1} S_1}{k} r \right) \quad (49)$$

$$R_{03} \left(\frac{\alpha_{n1} S_2}{k} r \right) = C_{1n} \cdot E_{2n} \cdot I_0 \left(\frac{\alpha_{n1} S_2}{k} r \right) + D_{1n} \cdot F_{2n} \cdot K_0 \left(\frac{\alpha_{n1} S_2}{k} r \right) \quad (50)$$

$$R_{04}(\alpha_{n1} r) = C_{1n} \cdot P_{1n} \cdot I_0(\alpha_{n1} r) + D_{1n} \cdot Q_{1n} \cdot K_0(\alpha_{n1} r) \quad (51)$$

since R_{0i} ($i = 1, 2, 3, 4$) satisfy the Bessel functions and the prime and double-prime over R_{0i} indicate the first and second differentiation with respect to its argument, respectively.

5. Thermal stresses in the isotropic cylinder

For an isotropic material, the elastic constants are written as follows

$$C_{11} = C_{33} = \bar{\lambda} + 2\bar{\mu}, \quad C_{12} = C_{13} = \bar{\lambda}, \quad C_{44} = \frac{1}{2}(C_{11} - C_{12}) = \bar{\mu} \quad (52)$$

where $\bar{\lambda} = \frac{E\nu}{(1+\nu)(1-2\nu)}$, $\bar{\mu} = \frac{E}{2(1+\nu)}$ (Lame's constants), E, ν are the Young's modulus and Poisson's ratio, respectively. also

$$\alpha_r = \alpha_z = \bar{\alpha} \text{ (say)}, \quad \beta_1 = \beta_2 = (3\bar{\lambda} + 2\bar{\mu})\bar{\alpha}, \quad k = 1 \quad (53)$$

In order to derive displacement and stress components of the isotropic cylinder, μ, S, λ which were determined for the anisotropic cylinder, must be defined, firstly.

Substituting constants (52), (53), to Eq. (33), we will have $\mu = 0$, then from Eqs. (31) and (32)

$$\bar{P}_n = \bar{Q}_n = \alpha_{n2}^{-2} \frac{3\bar{\lambda} + 2\bar{\mu}}{\bar{\lambda} + \bar{\mu}} \bar{\alpha} \quad (54)$$

and so on, using constants (52) and Eq. (35), the values of S, λ will be unity, then $\lambda_1 = \lambda_2 = 1$, $S_1 = S_2 = 1$. Therefore, Eq. (36) has one solution for the isotropic cylinder.

Accordingly, the Eq. (42) to Eq. (51), reduce to the isotropic equations as follows

$$\bar{u}(r, z) = \sum_{n=1}^{\infty} \alpha_{n2} [\bar{R}'_{02}(\alpha_{n2}r) + \bar{R}'_{04}(\alpha_{n2}r)] \sin(\alpha_{n2}z) \quad (55)$$

$$\bar{w}(r, z) = \sum_{n=1}^{\infty} \alpha_{n2} [\bar{R}_{02}(\alpha_{n2}r)] \cos(\alpha_{n2}z) \quad (56)$$

$$\begin{aligned} \bar{\sigma}_{rr} = \bar{\eta} \sum_{n=1}^{\infty} \alpha_{n2}^2 \{ (1 - \nu) [\bar{R}''_{02}(\alpha_{n2}r) + \bar{R}''_{04}(\alpha_{n2}r)] \\ + \nu [(\alpha_{n2}r)^{-1} [\bar{R}'_{02}(\alpha_{n2}r) + \bar{R}'_{04}(\alpha_{n2}r)] - \bar{R}_{02}(\alpha_{n2}r)] \\ - (1 + \nu) \alpha \bar{R}_{01}(\alpha_{n2}r) \} \sin(\alpha_{n2}z) \end{aligned} \quad (57)$$

$$\begin{aligned} \bar{\sigma}_{\theta\theta} = \bar{\eta} \sum_{n=1}^{\infty} \alpha_{n2}^2 \{ (1 - \nu) (\alpha_{n2}r)^{-1} [\bar{R}'_{02}(\alpha_{n2}r) + \bar{R}'_{04}(\alpha_{n2}r)] \\ + \nu \left[[\bar{R}''_{02}(\alpha_{n2}r) + \bar{R}''_{04}(\alpha_{n2}r)] - \bar{R}_{02}(\alpha_{n2}r) \right] \\ - (1 + \nu) \alpha \bar{R}_{01}(\alpha_{n2}r) \} \sin(\alpha_{n2}z) \end{aligned} \quad (58)$$

$$\begin{aligned} \bar{\sigma}_{zz} = \bar{\eta} \sum_{n=1}^{\infty} \alpha_{n2}^2 \{ \nu [[R''_{02}(\alpha_{n2}r) + R''_{04}(\alpha_{n2}r)] + (\alpha_{n2}r)^{-1} [R'_{02}(\alpha_{n2}r) + R'_{04}(\alpha_{n2}r)]] \\ - (1 - \nu) R_{02}(\alpha_{n2}r) - (1 + \nu) \alpha R_{01}(\alpha_{n2}r) \} \sin(\alpha_{n2}z) \end{aligned} \quad (59)$$

$$\bar{\tau}_{rz} = \bar{\mu} \sum_{n=1}^{\infty} \alpha_{n2}^2 \{ R'_{02}(\alpha_{n2}r) + R'_{04}(\alpha_{n2}r) \} \cos(\alpha_{n2}z) \quad (60)$$

in which

$$\bar{R}_{01}(\alpha_{n2}r) = C_{2n} \cdot I_0(\alpha_{n2}r) + D_{2n} \cdot K_0(\alpha_{n2}r) \quad (61)$$

$$\bar{R}_{02}(\alpha_{n2}r) = C_{2n} \cdot \bar{E}_{1n} \cdot I_0(\alpha_{n2}r) + D_{2n} \cdot \bar{F}_{1n} \cdot K_0(\alpha_{n2}r) \quad (62)$$

$$\bar{R}_{04}(\alpha_{n2}r) = 2(1 + \nu) \alpha_{n2}^{-2} [C_{2n} \cdot I_0(\alpha_{n2}r) + D_{2n} \cdot K_0(\alpha_{n2}r)] \quad (63)$$

$$\bar{\eta} = \frac{E}{(1 + \nu)(1 - 2\nu)}$$

6. Mechanical boundary conditions

The mechanical boundary conditions are given by

$$u(r, z) = \bar{u}(r, z) = 0 \quad z = 0, \quad z = L \tag{64}$$

$$\sigma_{zz}(r, z) = \bar{\sigma}_{zz}(r, z) = 0 \quad z = 0, \quad z = L \tag{65}$$

$$\sigma_{rr}(r, z) = 0, \sigma_{rz}(r, z) = 0 \quad r = r_1 \tag{66}$$

$$\bar{\sigma}_{rr}(r, z) = 0, \bar{\sigma}_{rz}(r, z) = 0 \quad r = r_3 \tag{67}$$

$$\begin{aligned} \sigma_{rr}(r, z) &= \bar{\sigma}_{rr}(r, z) & r = r_2, \\ \sigma_{rz}(r, z) &= \bar{\sigma}_{rz}(r, z) & r = r_2 \end{aligned} \tag{68}$$

It is evident that the conditions (64) is satisfied automatically and the constants $E_{1n}, F_{1n}, E_{2n}, F_{2n}, \bar{E}_{1n}, \bar{F}_{1n}$ are determined, applying conditions (66)-(68).

7. Results and discussions

To present numerical results, we consider a hollow cylinder composed of Alumina (anisotropic) and 15Mo3 (isotropic) which is similar to a V94.2 gas turbine combustion chamber. The geometric

Table 1 Thermoelastic properties of Alumina and 15Mo₃

Thermoelastic properties	Alumina	15Mo ₃
Thermal expansion coefficient (10 ⁻⁶ k ⁻¹) (Eslami and Hetnarski 2013)	$\alpha_r = 8.3, \quad \alpha_z = 9$	$\alpha = 13$
Young's modulus (GPa)	-	190
Poisson's ratio	-	0.29
Elastic constants (GPa) (Lenkhmitskii 1981)	$C_{11} = 460.2, \quad C_{12} = 174.7, \quad C_{13} = 127.4,$ $C_{33} = 509.5, \quad C_{44} = 126.9$	-

Table 2 Thermal properties of internal and external flow*

Thermoelastic properties	Internal flow	External flow
Fluid temperature (°k)	$T_\infty = 1600$	$T_0 = 623$
Convective coefficient (w/m ² k)	$h_1 = 106$	$h_2 = 273$
Radiative heat rate (w/m ²)	$q_1'' = 11000$	$q_2'' = 3000$

*These parameters are estimated using equations which are given in Barsoum (2003)

parameters are $r_1 = 1.1 \text{ m}$, $r_2 = 1.14 \text{ m}$, $r_3 = 1.16 \text{ m}$ and $L = 2.321 \text{ m}$. The value of k has been taken to be unity for anisotropic material (Alumina). Thermo-elastic properties of Alumina and 15Mo3 as well as thermal conditions are given in Tables 1 and 2, respectively.

Fig. 2 shows the numerical results of the steady-state temperature distribution at the inner and outer surfaces for the various values of thermal conductivity ratio k_3 in the z -direction. It is found that due to the axisymmetric thermal boundary conditions, the maximum value of the temperature is occurred at the middle area of the cylinder. It also can be seen that the internal and external surface temperatures as well as the temperature difference between them increases as the thermal conductivity ratio enhances. In particular, for $k_3 = 0.5$ inside and outside temperatures are very close to each other. Because in this case the rate of conduction heat transfer in the isotropic cylinder increases compared to the anisotropic cylinder.

Fig. 3 illustrates the numerical results of the temperature at the middle point of the hollow cylinder through the thickness direction for $k_3 = 1$. It is observed that due to the homogeneity of

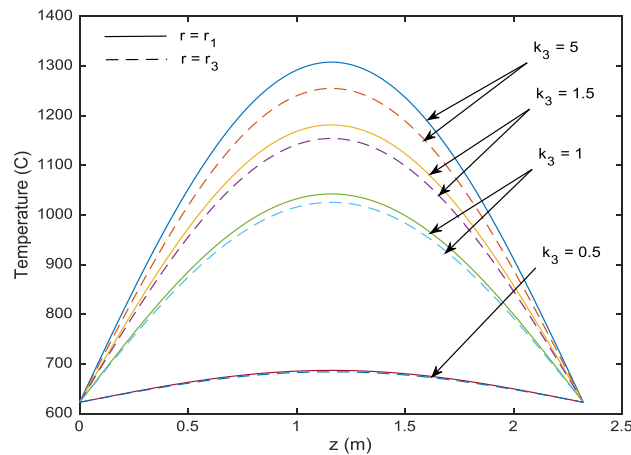


Fig. 2 Temperature distribution at the inner and outer surfaces for various values of k_3

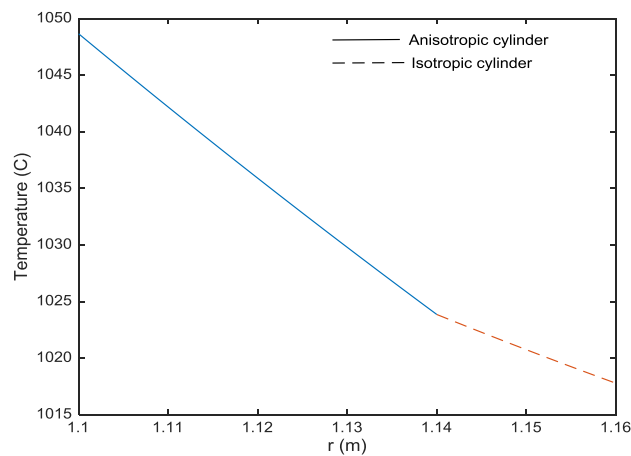


Fig. 3 Temperature distribution in r -direction for $z = L/2$ and $k_3 = 1$

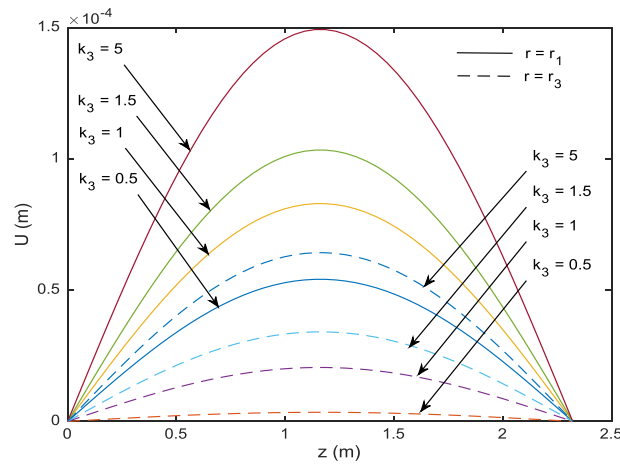


Fig. 4 Radial displacement at the inner and outer surfaces for various values of k_3

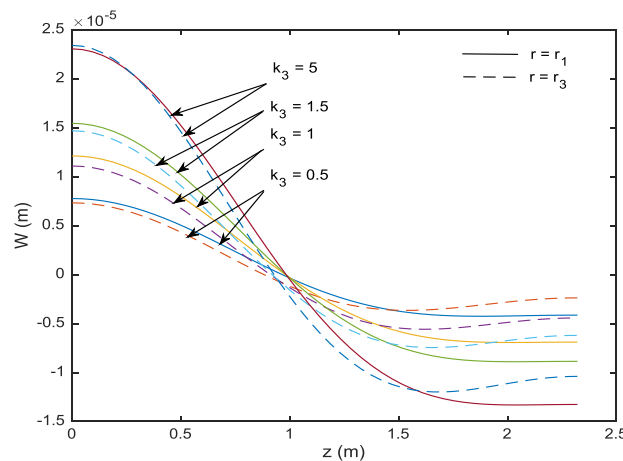


Fig. 5 Axial displacement at the inner and outer surfaces for various values of k_3

the materials the variations of the temperature are linear. It is also shown that the temperature distribution is continuous at the contact surface and the temperature reduces as the radius increases which corresponds to the direction of heat transfer in the cylinder and the temperature reduction rate is more quickly in the anisotropic cylinder than the isotropic cylinder.

Figs. 4 and 5 show the numerical results of the radial and axial displacements, respectively. It is found that the radial displacement is axisymmetric in the z -direction and its maximum value is taken place at the middle area of the cylinder while the axial displacement is not axisymmetric and reaches its maximum values at the lower face of cylinder. It is also noticeable that the thermal conductivity ratio changes are more affected the radial displacement which this effect is more in the anisotropic cylinder than the isotropic cylinder, in turn.

Figs. 6-8 present the axial variation of the radial, hoop and axial thermal stress distributions at the inner and outer surfaces of the composite hollow cylinder for the various values of thermal conductivity ratio. It is shown that the stress magnitudes are increased as the thermal conductivity

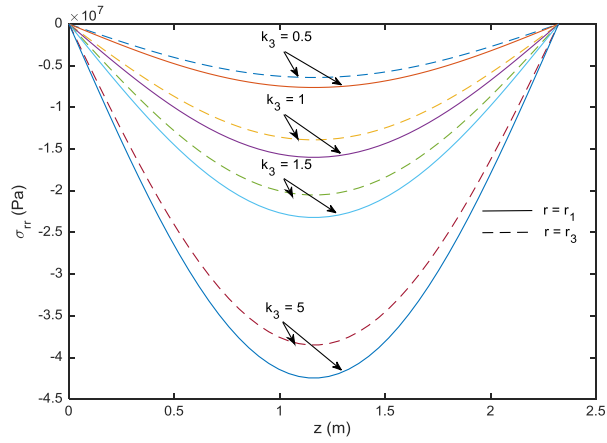


Fig. 6 Radial stress distribution at the inner and outer surfaces for various values of k_3

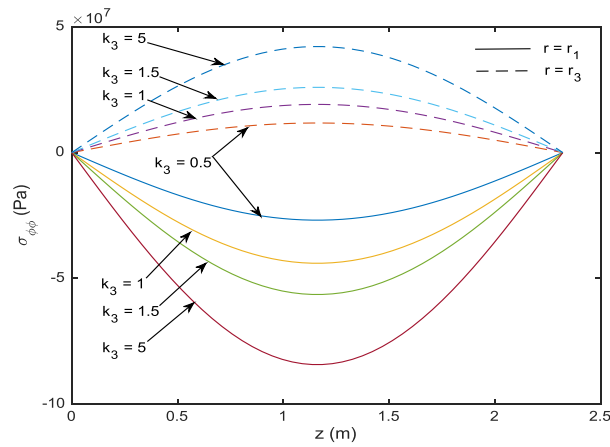


Fig. 7 Hoop stress distribution at the inner and outer surfaces for various values of k_3

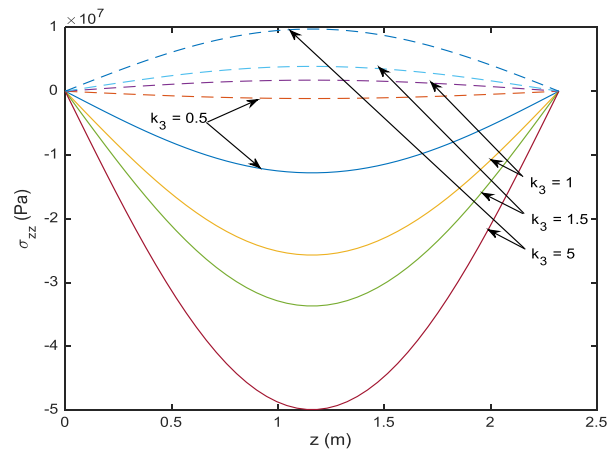


Fig. 8 Axial stress distribution at the inner and outer surfaces for various values of k_3

ratio (k_3) is increased. It is also found that the radial stress is compressive at the internal and external surfaces while the hoop stress is compressive at the interface and tensile at the outer surface. As discussed in Chen and Chu (1989), this situation is due to the thermal expansion of the inner part of the cylinder which is constrained by the outer part and both ends of the cylinder but the outer surface is constrained by both ends of the cylinder only. When heat is applied at the inner surface, the radial stress is compressive at the inner and outer surfaces while the hoop stress is compressive at the inner part of the cylinder and tensile at the outer surface. But this condition is different for the axial stress. As shown in Fig. 8 the axial stress is compressive at the internal surface, however, at the outer surface depending on the values of the thermal conductivity ratio can be compressive or tensile. It is further noted that the values of radial, hoop and axial stresses in the isotropic cylinder are less than the anisotropic cylinder.

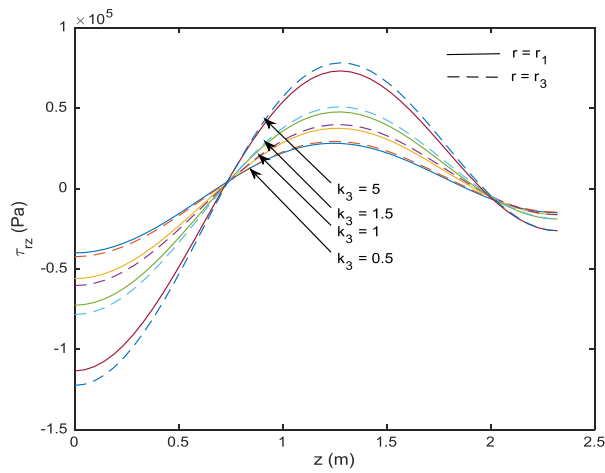


Fig. 9 Shear stress distribution at the inner and outer surfaces for various values of k_3

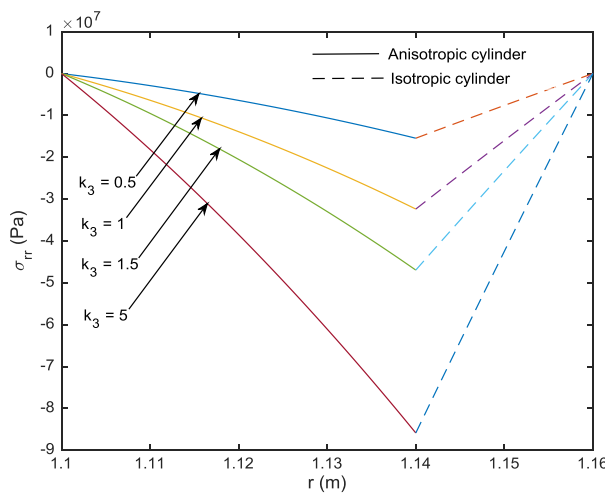


Fig. 10 Radial stress distribution in r-direction for $z = L/2$

Fig. 9 illustrates the shear stress distribution in the axial direction. It is found that the distribution of this stress isn't axisymmetric and its values are increased as the thermal conductivity ratio is increased. It also can be shown that the maximum value of the shear stress is occurred at the lower face.

Fig. 10 shows the radial stress distribution in the r-direction of cylinder. As regards, the temperature distribution is linear in this direction, it can be seen that the radial stress is linear too, approximately. It also shows that the radial stress is compressive in the thickness direction and its magnitude is increased to the contact surface of two cylinders, then reduced to the outer surface of the isotropic cylinder. This case can be explained refer to Fig. 4. As this fig shows, the values of radial displacement in the inner part are more than the outer part, then the anisotropic cylinder which is constrained by isotropic cylinder will be under compressive stress.

8. Conclusions

Many researches have analyzed the temperature and thermal stress distributions in cylinders, but a cylinder which is composed of anisotropic and isotropic materials hasn't considered, yet. This persuade us to study this issue because of its importance in major industries such as power plants. Therefore, in this paper developed an analytical solution for the steady-state axisymmetric thermal stress distributions in a composite anisotropic and isotropic hollow cylinder. A method based on the Bessel functions and Potential function displacements is developed to obtain numerical results.

The main conclusions are as follows:

- The temperature and thermal stresses increases as the thermal conductivity ratio increases and the maximum values of them occurred in the middle area of the hollow cylinder.
- The radial stress is compressive at the internal and external surfaces while the hoop stress is compressive at the interface and tensile at the outer surface.
- The axial stress is compressive in the internal surface but in the outer surface depending on the values of the thermal conductivity ratio can be compressive or tensile.
- The temperature and thermal stress distributions are linear through the thickness direction and decreases from the internal surface of anisotropic cylinder to the outer surface of isotropic cylinder, however, the decreasing rate in anisotropic cylinder is more than the isotropic cylinder.
- The values of the radial, hoop and axial stress in the anisotropic cylinder are more than the isotropic cylinder.

It is worthy to note that the values of the thermal conditions which estimated in this research, not to be presented in any other papers but they are very accurate in calculation.

Acknowledgments

The authors would like to thank the referees for their valuable comments. Also, they are thankful to thank the University of Kashan for supporting this work by Grant No. 682561/5.

References

- Aziz, A. and Torabi, M. (2013), "Thermal stresses in a hollow cylinder with convective boundary conditions on the inside and outside surfaces", *J. Thermal. Stress.*, **36**(10), 1096-1111.
<https://doi.org/10.1080/01495739.2013.818894>
- Bamdad, M., Mohammadimehr, M. and Alambeigi, K. (2019), "Analysis of sandwich Timoshenko porous beam with temperature-dependent material properties: Magneto-electro-elastic vibration and buckling solution", *J. Vib. Control*, **25**(23-24), 2875-2893. <https://doi.org/10.1177/1077546319860314>
- Barsoum, M.W. (2003), *Fundamentals of Ceramics*, IOP, Oxford, UK.
- Bensaid, I. and Bekhadda, A. (2018), "Thermal stability analysis of temperature dependent inhomogeneous size-dependent nano-scale beams", *Adv. Mater. Res., Int. J.*, **7**(1), 1-16.
<https://doi.org/10.12989/amr.2018.7.1.001>
- Chen, L.S. and Chu, H.S. (1989), "Transient thermal stresses of a composite hollow cylinder heated by a moving line source", *Comput. Struct.*, **33**(5), 1205-1214. [https://doi.org/10.1016/0045-7949\(89\)90459-8](https://doi.org/10.1016/0045-7949(89)90459-8)
- Dejean, T.T. and Mohr, D. (2018), "Elastically-isotropic elementary cubic lattices composed of tailored hollow beams", *Extrem. Mech. Lett.*, **22**, 13-18. <https://doi.org/10.1016/j.eml.2018.04.005>
- Eslami, R. and Hetnarski, R.B. (2013), *Theory of Elasticity and Thermal Stresses*, Springer, New York, USA.
- Ghorbanpour Arani, A., Rousta Navi, B. and Mohammadimehr, M. (2016), "Surface stress and agglomeration effects on nonlocal biaxial buckling polymeric nanocomposite plate reinforced by CNT using various approaches", *Adv. Compos. Mater.*, **25**(5), 423-441.
<https://doi.org/10.1080/09243046.2015.1052189>
- Jin, Zh.H. and Noda, N. (1994), "Transient thermal stress intensity factors for a crack in a semi-infinite plate of a functionally gradient material", *Int. J. Solid. Struct.*, **31**(2), 203-218.
[https://doi.org/10.1016/0020-7683\(94\)90050-7](https://doi.org/10.1016/0020-7683(94)90050-7)
- Lee, Z. (2005), "Hybrid Numerical Method Applied to 3-D Multilayered Hollow Cylinder with Periodic Loading Conditions", *App. Math. Comput.*, **166**, 95-117. <https://doi.org/10.1016/j.amc.2004.04.038>
- Lenkhnikskii, S.G. (1981), *Theory of Elasticity of an Anisotropic Body*, (2nd edition), MIR publishers, Moscow, Russia.
- Liu, Y.J. and Yin, H.M. (2014), "Elastic thermal stresses in a hollow circular overlay/ substrate system", *Mech. Research. Commun.*, **55**, 10-17. <https://doi.org/10.1016/j.mechrescom.2013.10.002>
- Mahmoudi, H. and Atefi, G. (2012), "Analytical solution for thermal stresses in a hollow cylinder under periodic thermal loading", *Proc. Inst. Mech. Eng., Pt. C: J. Mech. Eng. Sci.*, **226**(7), 1705-1724.
<https://doi.org/10.1177/0954406211429757>
- Misra, J.C. and Achari, R.M. (1980), "On Axisymmetric Thermal Stresses in an Anisotropic Hollow Cylinder", *J. Thermal. Stress.*, **3**(4), 509-520. <https://doi.org/10.1080/01495738008926986>
- Mohammadimehr, M. and Mehrabi, M. (2017), "Electro-thermo-mechanical vibration and stability analyses of double-bonded micro composite sandwich piezoelectric tubes conveying fluid flow", *Appl. Math. Model.*, **60**, 255-272. <https://doi.org/10.1016/j.apm.2018.03.008>
- Mohammadimehr, M. and Mehrabi, M. (2018a), "Stability and free vibration analyses of double-bonded micro composite sandwich cylindrical shells conveying fluid flow", *Appl. Math. Model.*, **47**, 685-709.
<https://doi.org/10.1016/j.apm.2017.03.054>
- Mohammadimehr, M. and Rostami, R. (2018b), "Bending and vibration analyses of a rotating sandwich cylindrical shell considering nanocomposite core and piezoelectric layers subjected to thermal and magnetic fields", *Appl. Math. Mech.*, **39**(2), 219-240. <https://doi.org/10.1007/s10483-018-2301-6>
- Mohammadimehr, M., Navi, B.R. and Arani, A.G. (2017), "Dynamic stability of modified strain gradient theory sinusoidal viscoelastic piezoelectric polymeric functionally graded single-walled carbon nanotubes reinforced nanocomposite plate considering surface stress and agglomeration effects under hydro-thermo-electro-magneto-mechanical loadings", *Mech. Adv. Mater. Struct.*, **24**(16), 1325-1342.
<https://doi.org/10.1080/15376494.2016.1227507>
- Moosaie, A. (2016), "A nonlinear analysis of thermal stresses in an incompressible functionally graded

- hollow cylinder with temperature-dependent material properties”, *Europ. J. Mech. A/Solid.*, **55**, 212-220.
<https://doi.org/10.1016/j.euromechsol.2015.09.005>
- Namayandeh, M.J., Mohammadimehr, M. and Mehrabi, M. (2019), “Temperature distribution of ceramic panels of a V94.2 gas turbine combustor under realistic operation conditions”, *Adv. Mater. Res., Int. J.*, **8**(2), 117-135. <https://doi.org/10.12989/amr.2019.8.2.117>
- Rajabi, J. and Mohammadimehr, M. (2019), “Hydro-thermo-mechanical biaxial buckling analysis of sandwich micro-plate with isotropic/orthotropic cores and piezoelectric/polymeric nanocomposite face sheets based on FSDT on elastic foundations”, *Steel. Compos. Struct., Int. J.*, **33**(4), 509-523.
<https://doi.org/10.12989/scs.2019.33.4.509>
- Shahedi, S. and Mohammadimehr, M. (2019), “Vibration analysis of rotating fully-bonded and delaminated sandwich beam with CNTRC face sheets and AL-foam flexible core in thermal and moisture environments”, *Mech. Based. Design. Struct. Mach.*, pp. 1-31.
<https://doi.org/10.1080/15397734.2019.1646661>
- Shahedi, S. and Mohammadimehr, M. (2020), “Nonlinear high-order dynamic stability of AL-foam flexible cored sandwich beam with variable mechanical properties and carbon nanotubes-reinforced composite face sheets in thermal environment”, *J. Sandw. Struct. Mater.*, **22**(2), 248-302.
<https://doi.org/10.1177/1099636217738908>
- Xue, Z.N., Chen, Z.T. and Tian, X.G. (2018), “Transient thermal stress analysis for a circumferentially cracked hollow cylinder based on memory-dependent heat conduction model”, *Theory. Appl. Frac. Mech.*, **96**, 123-133. <https://doi.org/10.1016/j.tafmec.2018.04.008>
- Yaragal, S.C. and Ramanjaneyulu, S. (2016), “Exposure to elevated temperatures and cooled under different regimes—a study on polypropylene concrete”, *Adv. Mater. Res., Int. J.*, **5**(1), 21-34.
<https://doi.org/10.12989/amr.2016.5.1.021>
- Yee, K.C. and Moon, T.J. (2002), “Plane thermal stress analysis of an orthotropic cylinder subjected to an arbitrary, transient, asymmetric temperature distribution”, *ASME, J. App. Mech.*, **69**, 632-640.
<https://doi.org/10.1115/1.1491268>
- Zenkour, A.M. (2014), “Exact solution of thermal stress problem of an inhomogeneous hydrothermal piezoelectric hollow cylinder”, *Appl. Math. Model.*, **38**, 6133-6143.
<https://doi.org/10.1016/j.apm.2014.05.028>
- Zibdeh, H.S. and Al Farran, J.M. (1995), “Stress analysis in composite hollow cylinders due to an asymmetric temperature distribution”, *J. Pressure. Vessel. Tech.*, **117**, 59-65.
<https://doi.org/10.1115/1.2842091>